Thermally-activated cation ordering in ZnGa$_2$Se$_4$ single crystals studied by Raman scattering, optical absorption, and ab initio calculations

R. Vilaplana,[1] O. Gomis,[1] E. Pérez-González,[2] H.M. Ortiz[3†], F.J. Manjón,[4,*]
P. Rodríguez-Hernández,[2] A. Muñoz,[2] P. Alonso-Gutiérrez[5], M.L. Sanjuán[5],
V.V. Ursaki[6] and I.M. Tiginyanu[6]

[1] *Centro de Tecnologías Físicas: Acústica, Materiales y Astrofísica, MALTA Consolider Team, Universitat Politècnica de València, 46022 València, Spain*

[2] *Departamento de Física Fundamental II, Instituto de Materiales y Nanotecnología, MALTA Consolider Team, Universidad de La Laguna, 38205 Tenerife, Spain*

[3] *Proyecto Curricular Licenciatura en Física, Universidad Distrital "Fco. José de Caldas", Bogotá, Colombia*

[4] *Instituto de Diseño para la Fabricación y Producción Automatizada, MALTA Consolider Team, Universitat Politècnica de Valencia, 46022 Valencia, Spain*

[5] *Instituto de Ciencia de Materiales de Aragón, (C.S.I.C. - Universidad de Zaragoza),Dept. Física de la Materia Condensada, Universidad de Zaragoza, 50009 Zaragoza, Spain*

[6] *Institute of Applied Physics, Academy of Sciences of Moldova, 2028 Chisinau, Moldova*

†On leave from CINVESTAV, Departamento de Nanociencia y Nanotecnología (Zacatenco, México D.F.), Unidad de Querétaro, Querétaro, México

Abstract

Order-disorder phase transitions induced by thermal annealing have been studied in the ordered-vacancy compound ZnGa$_2$Se$_4$ by means of Raman scattering and optical absorption measurements. The partially disordered as-grown sample with tetragonal defect stannite (DS) structure and *I*-42m space group has been subjected to controlled heating and cooling cycles. *In situ* Raman scattering measurements carried out during the whole annealing cycle show that annealing the sample to 400ºC results in a cation ordering in the sample leading to the crystallization of the ordered tetragonal defect chalcopyrite (DC) structure with *I*-4 space group. On decreasing temperature the ordered cation scheme of the DC phase can be retained at ambient conditions. The symmetry of the Raman-active modes in both DS and DC phases is discussed and the similarities and differences between the Raman spectra of both phases emphasized. The ordered structure of annealed samples is confirmed by optical absorption measurements and *ab initio* calculations that show that the direct bandgap of DC-ZnGa$_2$Se$_4$ is larger than that of DS-ZnGa$_2$Se$_4$.

* Corresponding author: fjmanjon@fis.upv.es

1. INTRODUCTION

Zinc digallium selenide ($ZnGa_2Se_4$) is one of the most studied, and probably one of the most controversial semiconductors of the adamantine-type tetrahedrally-coordinated $A^{II}B_2^{III}X_4^{VI}$ family of ordered-vacancy compounds (OVCs). OVCs derive from the diamond and the zincblende or sphalerite (F-43m) structure and have a vacant cationic site in an ordered and stoichiometric fashion; i.e., a stoichiometric vacancy is located at a fixed Wyckoff position in the unit cell [1]. A common trend in all adamantine OVCs is that they have several non-equivalent tetrahedrally-coordinated cations resulting in a distortion of the crystal lattice from the cubic symmetry. The lack of cubic symmetry provides special properties to this family of semiconductors with important applications in optoelectronics, solar cells, and non-linear optics that has been considerably reviewed [1-4]. In particular, $ZnGa_2Se_4$ has a high photosensitivity and strong luminescence [2]. There is a recent great interest in the applications of the OVCs properties, and $ZnGa_2Se_4$ has been proposed as a candidate to phase change memories to replace flash memories [5] and as a candidate for electronic device applications forming part of heterojunction diodes [6].

From the theoretical point of view, OVCs are also important materials in Solid State Physics because they allow us to understand the role played by vacancies in the physical and chemical properties of solids since they constitute a bridge between perfect materials (with no vacancies at all) and defect materials (with vacancies as point defects). Additionally, OVCs are of interest due to the order-disorder phase transitions occurring in tetrahedral semiconductors. In this sense, the properties of $ZnGa_2Se_4$ have been characterized by x-ray diffraction (XRD) [7,8], neutron and electron diffraction [9-12], extended x-ray absorption fine structure [13], infrared (IR) [14,15], Raman spectroscopy [15-24], and magnetic [25] measurements.

All the above techniques have been applied to resolve the structure of $ZnGa_2Se_4$; however, there is still a controversy about the real structure of $ZnGa_2Se_4$ at ambient conditions. Some authors claim that $ZnGa_2Se_4$ crystallizes in the tetragonal defect chalcopyrite (DC) structure with space group (S.G.) I-4 [see **Fig. 1(a)**] where cations and vacancies are completely ordered [7,13,15,16,22]. On the other hand, other authors report various degrees of cation disorder and claim that $ZnGa_2Se_4$ crystallizes in the tetragonal defect stannite (DS) structure, also known as defect famatinite, with S.G. I-42m and higher symmetry than the DC phase [8-12,21,26] [see **Fig. 1(b)**]. Unfortunately, the structure of $ZnGa_2Se_4$ at ambient conditions is difficult to identify by

x-ray diffraction because Zn and Ga atoms have similar x-ray scattering factors and both S.G. *I*-4 and *I*-42m have the same crystallographic extinctions. Consequently, neutron scattering measurements are more suitable to determine the crystalline structure of this compound since the coherent nuclear scattering lengths of these two atoms are not so similar.

As observed in **Fig. 1**, the DC and DS structures proposed in the literature for $ZnGa_2Se_4$ are very similar. In the DC structure, Ga atoms occupy *2a* and *2c* Wyckoff sites while vacancies and Zn atoms occupy *2b* and *2d* Wyckoff sites, respectively [see **Fig. 1(a)**]. If cations undergo a partial or total disorder different disordered structures may result **[27]**. The most frequent partially-disordered structure that $ZnGa_2Se_4$ adopts is the DS structure. It has been already discussed that there are several types of DS polytypes (models 1 to 5) depending on the interchange between cations and vacancies **[15,27,28]**. Most recent measurements suggest that $ZnGa_2Se_4$ adopts model 2 of the DS structure **[8,9]** (see table II in Ref. **27**). In model 2 of the DS structure, Zn atoms at *2d* sites of the DC phase and Ga atoms at *2c* sites of the DC phase substitute each other resulting in a fractional occupation of the *4d* Wyckoff site in the DS phase [see **Fig. 1(b)**]. At the same time, Ga atoms and vacancies at *2a* and *2b* sites in the DC phase, respectively, remain in the same lattice positions as in DC structure **[27]**.

The discrepancy about the structure of $ZnGa_2Se_4$ at ambient conditions has led to considerable misunderstanding of its properties, like the optical bandgap of the material or the frequencies and symmetries of the Raman-active modes **[15-24]**. Most of the difficulties to understand the structure of $ZnGa_2Se_4$ and consequently its properties come from the fact that most of the studies reported in the literature do not give detailed information of the crystal growth and the preparation of the studied samples. It is well-known that many semiconductors and their alloys undergo solid-solid phase transitions from ordered to disordered structures on increasing temperature above a critical value. In this respect, phase diagram studies reveal that several order–disorder transitions at relatively low temperatures are present in $ZnGa_2Se_4$ **[16,25,29]**. It has been recently evidenced that details of crystal growth and sample preparation, like the maximum temperature reached in post-growth annealing treatment, or the rate of decrease of temperature during the growth process or the annealing treatment are crucial points allowing one to understand the final structure of this compound at ambient conditions **[24,25]**.

In this study, we report Raman scattering and optical absorption measurements in $ZnGa_2Se_4$ samples to study the thermally-induced order-disorder processes occurring in this interesting semiconductor. We show that moderate annealing of DS- $ZnGa_2Se_4$ to 400°C followed by a controlled and slow cooling process results in the growth of DC-$ZnGa_2Se_4$ with different properties than those of original DS-$ZnGa_2Se_4$.

2. EXPERIMENTAL DETAILS

The disorder of the DC structure with the increase of the Zn content has been studied carefully on $Zn_{1-x}Mn_xGa_2Se_4$ samples [10-12,30]. In this context, Raman studies on initially DS-$Zn_{0.5}Mn_{0.5}Ga_2Se_4$ samples subjected to different thermal treatments have revealed that a thermally-induced order occurs above 250 °C leading to a perfect DC structure; however, upon further heating this material undergoes an order-disorder phase transition from the DC structure to a DS structure (that maintains the ordered stoichiometric vacancies) with Tc close to 500 °C [24]. Furthermore, cooling at slow rates across the phase transition allows the sample to reach at room temperature (RT) an almost fully ordered configuration as expected in the DC structure; however, fast cooling rates may freeze a metastable configuration resulting in the DS structure [16,24,25]. A recent x-ray analysis, where the magnetic properties of the $Zn_{1-x}Mn_xGa_2Se_4$ were studied, revealed that $ZnGa_2Se_4$ crystallizes in S.G. *I*-4 when a careful crystal growth process is carried out where annealing to equilibrium at a suitable temperature is followed by slow cooling to RT [25]. In other words, the above mentioned studies show that due to the relative low temperature of the order–disorder phase transition (~ 470 °C in $ZnGa_2Se_4$) a complete positional order of the cations may not be easy to achieve during the cooling process of the samples, and this is the reason why the crystal of $ZnGa_2Se_4$ may retain the high-temperature disordered phase *I*-42m at RT. Therefore, the discrepancy about the crystallographic structure of $ZnGa_2Se_4$ at RT and normal pressure in the literature could be related with the sample preparation process.

For this study, DS-$ZnGa_2Se_4$ crystals were grown from its constituents ZnSe and Ga_2Se_3 by chemical vapor transport method using iodine as a transport agent [31] and are the same used previously in Raman scattering measurements [21] and in a structural study under pressure by means of XRD measurements [8]. On the other hand, DC-$ZnGa_2Se_4$ crystals were obtained from as-grown DS-$ZnGa_2Se_4$ by subjecting them to controlled heating and cooling cycles in vacuum, following the procedure described in

Ref. **24**. In a first run, samples were heated at 400ºC during 1 hour and cooled to ambient temperature at a rate of 1ºC/min. After cooling, structural order had increased but the degree of cation order, as measured by the ratio of Raman bands characteristic of *I*-4 and *I*-42m phases, was still low. A second cycle of 8h heating at 300ºC followed by slow cooling at the same rate of 1ºC/min did not improve order. Finally, a third annealing process was conducted where the sample was held for 10 h at 400ºC and then slowly cooled at 1ºC/min. This resulted in the crystallization of the sample in the DC phase though some small partial cation disorder remains.

Raman scattering measurements were performed in backscatter geometry with either a LabRAM HR UV microspectrometer coupled to a Peltier-cooled CCD camera (unpolarized measurements) or a Dilor XY spectrometer with a liquid-nitrogen cooled CCD camera (polarized measurements). In both measurements a 632.81 nm (1.96 eV) HeNe laser excitation line with a power around 1 mW and a spectral resolution better than 2 cm^{-1} were used. In order to perform the laser annealing and *in situ* Raman measurements the samples were placed into a Linkam T1500 stage under vacuum of 10^{-5} Torr. During Raman experiments, samples were checked before and after each measurement in order to be sure that no heating effects occur during the measurements by the incoming laser excitation. In order to analyze the Raman spectra, Raman peaks have been fitted to a Voigt profile (Lorentzian profile convoluted by a Gaussian profile) where the spectrometer resolution is taken as a fixed Gaussian width. On the other hand, optical absorption measurements in both DS- and DC- ZnGa$_2$Se$_4$ samples were performed at room temperature by the sample-in sample-out method using a micro-optical system **[32]** in combination with a tungsten lamp and an Ocean Optics spectrometer.

3. *AB INITIO* CALCULATIONS

Total energy calculations were performed within the framework of the density functional theory (DFT) and the pseudopotential method using the Vienna *ab initio* simulation package (VASP) of which a detailed account can be found in **[33]** and references therein. The exchange and correlation energy has been taken in the generalized gradient approximation (GGA) according to Perdew-Burke-Ernzerhof (PBE) prescription **[34]**. Details of total-energy calculations in the DC structure can be consulted in Refs. **27 and 35,** a plane wave cutoff of 520 eV and a k-mesh of (4,4,4) was used with the primitive cell. Total energy calculations were also performed for the

DS structure. Out of the five possible DS phases for OVCs discussed by Eifler *et al.* and Gomis *et al.* **[15,27,28]**, we have performed calculations for model 1 despite the fact that we consider that samples of the DS phase likely correspond to model 2 **[27]**. Note that in model 1 of the DS structure, all Ga atoms occupy *4d* sites, Zn atoms are in a *2a* site and vacancies are in *2b* sites, while in model 2 Zn and half Ga atoms are mixed in *4d* sites, the other half of Ga atoms are in *2a* sites and vacancies in *2b* sites.

We have tried to perform calculations for the DS phase model 2 with a supercell, but, unfortunately, these calculations become very time consuming and the symmetry of the structure after relaxation does not correspond to that of the original DS phase. In fact, for model 2 all the possible occupations of *4d* positions will change the symmetry to that of the I-4 structure or that of the two subgroups of the I-42m structure (S.G. 112, where *4d* sites transform to *2f* and *2e* sites, or S.G. 113, where *4d* sites transform to *2a* and *2b* sites). In this respect, we have also tried to perform calculations for the DS phase model 2 using the 112 and 113 subgroups of the I-42m structure which allow describing in two independent Wyckoffs the Zn and Ga atoms in the same cation plane perpendicular to the c axis. This method was recently used to simulate a high-pressure disordered spinel (S.G. 227) with an orthorhombic structure **[36]**. However, the number of phonons in these two subgroups is larger than in the DS structure and are not better than those of DS phase model 1 to interpret the Raman spectrum of DS-$ZnGa_2Se_4$.Therefore, for comparison purposes with the DS phase of $ZnGa_2Se_4$ we have decided to report the Raman-active mode of the DS phase model 1.

Initially lattice dynamics calculations of phonon modes were also performed with VASP in the DC and DS (model 1) structures **[27]** at the zone centre (Γ point) of the Brillouin zone (BZ). For that purpose, we calculated the dynamical matrix at the Γ point using the direct method **[37]**. This method involves a separate calculation of the forces in which a fixed displacement from the equilibrium configuration of the atoms within the primitive unit cell is considered. Details of the lattice dynamics calculations can be consulted in **Ref. 27**. Note that there is a different charge cationic sequence in the planes along the z axis for models 1 and 2 of the DS phase; e.g., the charges are 2x2=4 (z=0 plane) and 4x3=12 (z=0.25 plane) in model 1, while the charges are 2x3=6 (z=0 plane) and 2x5=10 (z=0.25 plane) in the model 2. Since electric dipoles in model 1 are larger than in model 2, we expect some differences between the vibrational properties of models 1 and 2 for DS-$ZnGa_2Se_4$. Therefore, the comparison of the experimental

Raman spectra and optical absorption of DS-ZnGa$_2$Se$_4$ (model 2) with theoretical calculations for model 1 are only approximate.

In order to include the LO-TO splitting in our study, we need to add the effect of the electric field that is not included in the previous direct force method. To obtain the LO-TO splitting with VASP we need to use the supercell method so that the dynamical matrix can be supplemented with a non-analytical term, which depends on the Born effective charge tensors and the electronic dielectric constant. With this approach, we did the calculation with VASP using different supercell sizes for one volume (or pressure) and found that the CPU time increased severely if an exact solution close to the Γ point is required. However, we checked that similar TO and LO phonon frequencies at the Γ point, but with a much less CPU time, were found using Density Functional Perturbation Theory (DFPT) [38] with the Quantum Espresso package [39]. In this software, we added the non-analytic term, due to the long-range interaction, using the response of the system to the electric field, which allows us to obtain the LO-TO splitting near the Γ point. Therefore, we can calculate the pure B and E modes with TO and LO splitting. In this context, we used ultrasoft pseudopotentials with a cutoff of 60 Ry and a k-mesh of (4 4 4) in order to obtain well converged results. Moreover, the same exchange correlation energy prescription was used in the total energy and lattice dynamics DFPT calculations. Therefore, in the following we will only present theoretical results for Raman-active modes including the LO-TO splitting based on DFPT with the Quantum Espresso package.

4. RESULTS AND DISCUSSION

A. Raman scattering measurements.

According to group theory [40], the DC structure of ZnGa$_2$Se$_4$ should have 21 vibrational modes at Γ with the following mechanical representation:

$$\Gamma_{21}: 3A \oplus 6B \oplus 6E \qquad (1)$$

where A modes are non-polar modes, and B and E modes are polar modes, E modes being doubly degenerated. This results in a total of 13 Raman-active modes ($3A \oplus 5B \oplus 5E$) and 10 IR-active modes ($5B \oplus 5E$) since one B and one E are acoustic modes. On

the other hand, the DS structure of $ZnGa_2Se_4$ (assuming it corresponds to either models 1, 2, or 3, where the *2b* site is only occupied by the vacancy [27]) should have 21 vibrational modes at Γ with the following mechanical representation:

$$\Gamma_{21}: 2A_1 \oplus A_2 \oplus 2B_1 \oplus 4B_2 \oplus 6E \qquad (2)$$

where B_2 and E are polar modes, E modes being doubly degenerated. This results in a total of 12 Raman-active modes ($2A_1 \oplus 2B_1 \oplus 3B_2 \oplus 5E$) because the A_2 mode is silent, and 8 IR-active modes ($3B_2 \oplus 5E$) since one B_2 and one E are acoustic modes.

In addition, two different wavenumbers (Raman or IR) should be observed for each polar mode, due to the transversal-longitudinal optic (TO-LO) splitting. Consequently, taking into account the TO-LO splitting, up to twenty-three Raman-active modes should be observed in the DC phase while twenty modes should be observed in the DS phase [27].

On the other hand, we have to note that both DC and DS compounds are optically uniaxial, which means that, except for incidence along the optical axis or at 90º from it, symmetry or character coupling is to be expected [41,42]. Thus, one may observe either E, B or TO, LO quasimodes, resulting from coupling of $E_{TO}+E_{LO}$, $B_{TO}+B_{LO}$, $E_{TO}+B_{TO}$, or $E_{LO}+B_{LO}$, respectively, when Raman scattering is measured with laser incidence along the (111) plane depending on the relative magnitude of polar (LO-TO) versus anisotropy (B-E) splitting for each B-E pair of modes. From now on, we label the Raman modes with a letter, a subscript, and a superscript for the sake of clarity. The letter represents the symmetry of the mode, the subscript represents the different types of modes, and the superscript numbers them.

Figure 2 shows unpolarized Raman scattering spectra of $ZnGa_2Se_4$ during the third annealing process where the original DS sample was heated in vacuum till 400ºC, annealed at that temperature during 10 h and then slowly cooled down at a rate of 1ºC/min till room temperature (RT). It can be observed that after half an hour at 400ºC the original Raman spectrum of the DS phase (at bottom) remains basically the same but a small band around 225 cm^{-1} is clearly developed. Raman modes appear shifted to smaller wavenumbers due to heating. On increasing the time of annealing above 8 h it can be observed that the 225 cm^{-1} is more clearly defined, most of the Raman peaks sharpen, and also a strong band near 190 cm^{-1} develops. Finally, on cooling down to RT it can be observed that the Raman features developed because of annealing remained,

sharpened, and shifted to higher wavenumbers. In the following we will discuss the observed changes and we will propose that these changes in the Raman spectrum evidence the change from the DS to the DC structure in $ZnGa_2Se_4$.

Figure 3 shows unpolarized Raman scattering spectra of both DC- and DS-$ZnGa_2Se_4$ at ambient conditions with incidence along the (111) pseudocubic direction, which is the usual direction of crystal growth. The symmetry assigned to the different Raman modes is added to help in the comparison of the different Raman spectra of both DS and DC samples. **Figure 3** shows that Raman scattering spectra of both DC- and DS-$ZnGa_2Se_4$ at ambient pressure look similar but have remarkable differences. The most general difference between both spectra is that Raman peaks of the DC phase have slightly larger intensities and smaller linewidths than those of the DS phase. In both DS and DC samples, the Raman spectrum can be divided into three regions: (i) the low-frequency region below 130 cm^{-1}, (ii) the medium-frequency region between 130 and 220 cm^{-1}, and (iii) the high-frequency region above 220 cm^{-1}. In general, the modes in the low- and medium-frequency region are more intense than those in the high-frequency region. In particular, the most intense peak of the Raman spectrum of DC-$ZnGa_2Se_4$ (DS-$ZnGa_2Se_4$) is the A^1 (A_1^1) mode. This mode is called the "breathing" mode since it is associated to the symmetric oscillation of the anions against the stoichiometric vacancy.

For the DC phase, we have observed 14 Raman-active modes at ambient conditions (13 modes of the DC phase, and one disorder-activated extra mode, that we will comment later on). For the DS phase, we have measured 12 Raman-active modes at ambient pressure. In the DC (DS) phase, the B and E (B_1, B_2 and E) modes spread mainly along the low- and high-frequency regions, while the non-polar A (A_1) modes are located in the medium-frequency region.

Before starting to describe in more detail the results of the Raman scattering measurements performed in DC- and DS-$ZnGa_2Se_4$ we would like to make some additional comments regarding the Raman spectrum of DS-$ZnGa_2Se_4$ in **Fig. 3**. First of all, we must note that the number of Raman-active modes we have measured in DS-$ZnGa_2Se_4$ is comparable to those of previous measurements though in some cases our assignments differ from those of other authors (see **Table 1**). The similarity between both DS and DC structures is evidenced in the fact that only one A-type mode is lost when going from the DC to the DS structure (models 1, 2, and 3). We identify the A^2 mode of the DC phase as the one located near 190 cm^{-1}, which is absent in the DS

sample and which, according to polarization measurements and lattice dynamics calculations (see below), has A-type symmetry. Therefore, the relative decrease of the intensity of this mode with respect to the intensity of the strongest A^1 mode can be taken as a measure of the degree of the cation disorder in the DC structure leading to the DS structure.

We also want to comment that Raman spectra presented in this work may also look slightly different to those previously reported. This has two explanations: the first one is the high sensitivity of the $ZnGa_2Se_4$ spectrum to the excitation wavelength due to resonance effects [30]; the second one is the varying degree of structural disorder found in different works, depending on the synthesis method, as already commented. In this context, our spectra for the DS phase ($\lambda_{exc}= 633$ nm) could look much similar to those of Refs. 17 and 19 ($\lambda_{exc}= 647$nm) than to those of Refs. 15 ($\lambda_{exc}= 750$ nm) and 21 ($\lambda_{exc}= 514.5$ nm). On the other hand, our spectra for the DC phase could look more similar to that of Ref. 16 (both taken with $\lambda_{exc}= 633$ nm) than to those of Ref. 15 ($\lambda_{exc}= 750$ nm) and 22 ($\lambda_{exc}= 514.5$ nm). As regards the structural disorder, our figures 2 and 3 and figure 2 in Ref. 15 show clearly how different can be Raman spectrum of $ZnGa_2Se_4$ due to structural disorder. Similarities and differences of our Raman spectra and those of previous works will be discussed in detail from now on.

A.1. Raman spectrum of DS phase

We will begin by describing the symmetry assignment of the Raman-active modes for the DS sample. Assignment has been made by combining polarized Raman measurements and lattice dynamics calculations. When an unequivocal assignment has not been possible due to the poor resolution of the Raman spectra of the DS phase, calculations have helped to identify the symmetry of the modes. We have marked in **Fig. 3** with vertical lines the calculated frequencies of the Raman modes with pure A-, B_1-, B_2-, and E-symmetry for DS-$ZnGa_2Se_4$ using model 1 of the DS structure. TO and LO splitting for B_2 and E polar modes are noted with solid and dotted lines, respectively. It can be noted that, though calculations were performed for model 1 instead of model 2, there is a rather good agreement between the experimental and calculated frequencies in the low and medium-frequency regions with the exception of the polar $B_2{}^1$ mode (see below an explanation for this disagreement). However, the difference between experimental and calculated frequencies is rather large for the polar

modes in the high-frequency region. Note that the accuracy of calculated frequencies by DFT methods is below 5% but it can be larger for the DS phase since we are not using the right model. It is noteworthy also to comment that the calculated LO-TO splittings are relatively large only for the *B* and *E* modes with the highest frequencies; i.e., the B_2^3 and E^5 modes. **Table 1** summarizes the experimental and theoretical frequencies for the Raman modes of DS-ZnGa$_2$Se$_4$ which are compared to previous results of Ursaki *et al.* **[21]** obtained with the same DS samples and to previous results obtained by Alonso-Gutiérrez **[23]**. We will discuss in the following differences between our results, those of Ursaki *et al.*, and those of Alonso-Gutiérrez.

On the basis of the above considerations, we have assigned the four modes of the low-frequency region (below 130 cm^{-1}) to E^1, B_1^1, E^2, and B_2^1 in order of increasing wavenumber. This assignment is similar to that performed in **Ref. 23** (see **Table 1**); however, in that work authors gave an interchanged assignment of the B_2^1 and B_1^2 Raman modes. Our assignment is based on our theoretical calculations and is supported by the small (large) infrared oscillator strength measured for the first (second) *B* mode observed in DC-ZnGa$_2$Se$_4$ by Eifler *et al.* **[15]** (assuming that differences between the DS and DC phases are minor). Note that in the DS phase the B_2 modes are polar but the B_1 mode is not; thus, B_1 modes do not show LO-TO splitting unlike B_2 modes. Therefore, the larger infrared oscillator strength of the first mode in the DC phase gives support to the assignment to the first *B* mode in the DS phase to the B_2 symmetry.

As regards the Raman modes of the medium-frequency region (between 130 and 220 cm^{-1}), we have assigned the mode near 140 cm^{-1} to the A_1^1 mode like in **Refs. 21** and **23**. Furthermore, in agreement with the proposal made in **Refs. 23 and 24** for the Zn$_{1-x}$Mn$_x$Ga$_2$Se$_4$ series, we have assigned the mode around 180 cm^{-1} in DS-ZnGa$_2$Se$_4$ to the silent A_2 mode instead of to the E^3 mode as was proposed in Ref. **21**. The broad band around 180 cm^{-1} has a frequency almost coincident with that of the theoretically predicted silent A_2 mode, which should be absent in Raman spectrum of the DS structure. However, it is also known that many silent modes become Raman active as a consequence of structural disorder **[43]**. In fact, in a previous work on the Zn$_{1-x}$Mn$_x$Ga$_2$Se$_4$ series, a broad band appearing around 180 cm^{-1} in the Raman spectra of all compounds of the series, either with S.G. *I*-42m or *I*-4, was assigned to disorder-activated vibrations having a similar pattern as the A_2 mode **[44]**. The presence of this mode in the DC phase is likely motivated by some degree of disorder present in the DC samples, as will be discussed in the next paragraphs. With all these considerations we

have tentatively assigned this broad band near 180 cm^{-1} to the silent A_2 mode.

The assignment of the E^3 mode in the DS phase is non trivial. Our calculations, which tend to underestimate Raman frequencies, yield a frequency for that mode much higher than the previously assigned values. In order to help in the identification of this mode we have plotted in **Fig. 4** the RT Raman spectrum of DS and DC samples in crossed polarization, with incident and outgoing radiation along the (111) direction, and incident electric field close to the [110] direction. In this configuration A modes are minimized while E ones are maximized. A mode is clearly observed around 196 cm^{-1} in these spectra, which we have attributed to the E^3 mode in both DS and DC phases. In non-polarized spectra this mode is partially hidden by nearby modes (see **Fig. 3**). Finally, we have assigned the mode near 210 cm^{-1} to the A_1^2 mode in good agreement with previous works **[21]**.

As regards the Raman modes of the high-frequency region (above 220 cm^{-1}), we have assigned a mode near 229.3 cm^{-1} to the B_1^2 mode. A mode close to this frequency was attributed to a B_2 mode in **Ref. 23**. Support for our assignment is again given by the small infrared oscillator strength measured for this mode (at 222 cm^{-1} in DC-ZnGa$_2$Se$_4$) by Eifler *et al.* **[15]**. However, our calculated frequency for the B_1^2 mode is much higher than the experimental one. We attribute this anomaly to the use of model 1 instead of the real model 2 in the calculations.

Finally, we have assigned the four Raman modes with highest-frequency above 230 cm^{-1} to quasiTO and quasiLO modes with B_2 and E mixed symmetry, in agreement with **Ref. 23**. Polarization experiments have allowed us to distinguish the quasiTO and quasiLO components of the $(E^4+B_2^2)$ mixed modes, which are found at about 239.4 and 246.5 cm^{-1}, respectively. Similarly, we have assigned the modes near 260.4 cm^{-1} (not observed by Ursaki *et al.* **[21]**) and 286 cm^{-1} to the quasiTO and quasiLO modes arising from $(E^5+B_2^3)$ mixed modes, respectively. The assignment of the four last modes to quasiTO and quasiLO mixed modes, and not to pure E(TO), B(TO), E(LO) or B(LO), is due to the fact that we have measured in backscattering geometry with the incident and outgoing radiation along the (111) direction (see **Table I**). Furthermore, our assignment of the two modes of higher frequency in the DS phase to partial B_2 symmetry is in good agreement with the rather strong oscillator strength measured for these modes in DC-ZnGa$_2$Se$_4$ by Eifler *et al.* **[15]**.

A.2. Raman spectrum of DC phase

As regards the assignment of the Raman modes in the DC phase, we have marked at the bottom of **Fig. 3** with vertical lines the theoretical frequencies for DC-ZnGa$_2$Se$_4$ to help in the symmetry assignment. TO and LO splitting for B and E polar modes are noted with solid and dotted lines, respectively. As already commented for the DS phase, the calculated LO-TO splittings for DC-ZnGa$_2$Se$_4$ are relatively large only for the B and E modes with the highest frequencies; i.e., the B^5 and E^5 modes and, to a lesser extent, the B^4 and E^4 modes. This result allows to explain why LO-TO splitting are barely seen in low-frequency modes in many OVCs. **Table 2** summarizes the experimental and theoretical frequencies at ambient conditions for the Raman modes of DC-ZnGa$_2$Se$_4$, which are compared to previous results reported by Eifler *et al.* and Tiginyanu *et al.* [15,16]. In this sense, our Raman spectrum for DC-ZnGa$_2$Se$_4$ shows similar features to those observed in previous Raman works on DC-ZnGa$_2$Se$_4$ [15,16,23].

We have to note that neither our frequencies for DC-ZnGa$_2$Se$_4$ nor those of **Refs. 15, 16, and 23** compare well with those reported by Allakhverdiev *et al.* [22]. These authors report an extraordinary large width of the A^1 mode (even on pressure upstroke), while our Raman spectra for the DC phase and in previous works [15-21,23] show much smaller widths for this mode. Furthermore, this mode, whose frequency is around 142-143 cm^{-1} in this and other works, shows a frequency at room pressure near 152 cm^{-1} in **Ref. 22**. Similarly, the A^3 mode reported around 193 cm^{-1} in **Ref. 22** is observed near 208-210 cm^{-1} in ours and other works [15-21,23]. These results pose a serious concern regarding the quality of the samples studied in that work. Consequently, we are not going to make further comparison of our results for DC-ZnGa$_2$Se$_4$ with the Raman spectra of **Ref. 22**. In this respect, we must note that the value of the c/a ratio of the ZnGa$_2$Se$_4$ samples reported by Allakhverdiev *et al.* in Ref. **22** is almost 2. It is known that the c/a ratio in OVCs with DC structure is typically below 1.90 [45-49] while the c/a ratio of OVCs with DS structure is typically above 1.97 (1.98 for DS-ZnGa$_2$Se$_4$) [8,45,50]. Therefore, the high value of c/a in Allakhverdiev's samples suggests that their samples have a large disorder and therefore they are not consistent with their claim to have the DC structure but a very disordered DS structure.

In the following we will try to justify our assignments for the symmetry of the Raman modes observed in DC-ZnGa$_2$Se$_4$ (see **Fig. 3**). The first thing we can comment on is that there is a much better agreement between the theoretical and experimental frequencies of the Raman-active modes for the DC phase than for the DS phase. The

better agreement is found not only in the low- and medium-frequency regions but also in the high-frequency region where the experimental-theoretical absolute deviations are larger.

As regards the Raman modes of the low-frequency region, the agreement with calculations is remarkable and the symmetry assignment of the Raman modes in these regions (E^1, B^1, E^2, B^2) is similar to that previously found in the literature [15,16]. A similar situation occurs in the medium-frequency region, where the theoretically-predicted frequencies of the A^1 and E^3 modes match nicely with experimental values (see **Table 2**). The largest deviations of theoretical calculations from experiments in this region correspond to the A^2 and A^3 modes whose predicted (observed) frequencies are 183 (188) and 197 (208) cm^{-1}, respectively (see **Table 2**). We have assigned the Raman mode of 208 cm^{-1} to the non polar A^3 mode in rather good agreement with the measurements of Eifler *et al.* and Tiginyanu *et al.* [15,16]. A remarkable feature of the medium-frequency region is the assignment of the E^3 mode. As already commented, this mode is partially hidden by the near A^2 mode in DC-ZnGa$_2$Se$_4$ but it can be observed under crossed polarization (see **Fig. 4**).

Another curious feature of the Raman spectrum of the DC phase is that a broad band is observed at the low frequency side of the A^2 mode whose frequency at room pressure is around 180 cm^{-1}. We have attributed this broad band to the local vibrations of the Se (anion) with displacements similar to those of the A^2 mode but arising from disordered regions. This mode seems to be analogous to the disorder-activated silent A_2 mode of the DS phase. Its presence in the Raman spectrum of the DC phase indicates the presence of some remaining disorder in our DC samples. Alonso-Gutiérrez *et al.* have also observed this broad band in their study of Zn$_{1-x}$Mn$_x$Ga$_2$Se$_4$ and correlated the intensity of this band to the degree of long-range order [23,24,44]. At this point, it is interesting to compare our Raman spectra on both DS- and DC-ZnGa$_2$Se$_4$ samples at ambient conditions (see **Fig. 3**) with those reported by Eifler *et al.* in Fig. 2 of **Ref. 15**. That figure shows Raman spectra in different surface areas of a DC-ZnGa$_2$Se$_4$ sample where changes in the broad band at the low-energy side of the A^2 mode near 180 cm^{-1} can be clearly observed [15]. In that work, the top spectrum is quite similar to our spectrum for DC-ZnGa$_2$Se$_4$ showing a small broad band due to certain disorder. The middle spectrum shows a broadening of all bands and the broad band near the A^2 mode is of the same intensity of the A^2 mode indicating a strong disorder in this area of the sample. Finally, the bottom spectrum in **Ref. 15** shows no broad band near the A^2 mode,

thus indicating a completely ordered DC phase in this area of the sample. In conclusion, our Raman spectrum for DC-ZnGa$_2$Se$_4$ evidences the presence of a small residual disorder, which is typical in this type of samples as evidenced by other authors.

As regards the Raman modes of the high-frequency region, we can make symmetry assignments by following a similar reasoning as in the assignment of the Raman mode symmetries in DS-ZnGa$_2$Se$_4$ and by comparing the Raman spectrum of DC-ZnGa$_2$Se$_4$ with those of other defect chalcopyrites, like DC-MnGa$_2$Se$_4$ [23,44]. We have assigned the mode at 229 cm^{-1} to the B^3 mode in rather good agreement with Eifler *et al.* [15]. Finally, we have assigned all the modes above 230 cm^{-1} to the quasiTO and quasiLO modes resulting from the mixture of the E^4 and B^4 and of the E^5 and B^5 modes. In general these high-frequency modes were not assigned to mixtures of E and B modes in the previous literature despite the fact that they should show this mixed character except when measurements are performed along high symmetry directions, as already commented.

In summary, the main differences between the Raman scattering spectra of DC and DS phases at ambient conditions are: i) Raman modes of the DC phase are sharper than those of the DS phase, in good agreement with the higher cation order in the DC phase than in the DS phase; ii) the silent mode (A_2) is disorder-activated in the DS phase and remains as a broad band in the DC structure, indicating incomplete cation order; iii) three A modes are detected in the DC phase while only two A modes are detected in the DS phase.

B. Optical absorption measurements.

In this section we will show that additional support to the distinction between DC and DS-ZnGa$_2$Se$_4$ comes from the comparison of the optical absorption spectra of both phases. **Figure 5** shows the optical absorption spectra of DC and DS-ZnGa$_2$Se$_4$ at ambient conditions. The high value of the absorption coefficient, α, its steep increase with photon energy, hv, and the linear character of the (αhv)^2 vs. hv plot at high energies (not shown), are indicative of the direct allowed nature of the bandgap in both DC- and DS-ZnGa$_2$Se$_4$. It can be observed that the fundamental absorption edge of the DC phase is slightly shifted towards higher energies with respect to that of the DS phase. This shift results in an increase of the direct bandgap energy of 0.1 eV from the DS to the DC phase. Marks of the experimental bandgap energies appear at the bottom of the optical absorption spectra for both DC (2.41 eV) and DS (2.31 eV) phases. The larger bandgap

energy for the DC phase than for the DS phase is supported by our theoretical calculations according to which the DC phase has a theoretical bandgap energy of 1.51 eV while that of the DS phase (model 1) is of only 1.02 eV. We must note that the agreement between experiments and calculations is only qualitative since theoretical DFT calculations usually underestimate the direct bandgap energy and the shift that must be applied to the theoretical values to match the experimental ones depends on the crystalline structure.

The decrease of the direct bandgap energy in $ZnGa_2Se_4$ when going from the ordered DC to the partially cation disordered DS phase can be explained by the increase of cation disorder. In a previous high-pressure optical study of $DC-CdGa_2Se_4$, we reported a decrease of about 0.1 eV in the direct bandgap at the pressure-induced DC to DS phase transition [35]. Furthermore, in that work we reported that a decrease of the bandgap of 0.4 eV was measured when the sample transited to the fully cation-vacancy disordered zincblende (DZ) phase [35]. A similar but smaller decrease of the bandgap was also experimentally found in $CdGa_2Te_4$ where the disorder at cation sites causes the decrease of the bandgap energy from 1.5 eV in the ordered DC structure to 1.4 eV in the DZ phase [3]. Furthermore, a strong decrease of the direct bandgap energy was found in going from the ordered chalcopyrite structure to the DZ structure in several chalcopyrite-type compounds [51]. In this context, we interpret that the decrease of the direct bandgap energy in the DS phase of $ZnGa_2Se_4$ with respect to the DC phase is related to the increase of cation disorder that leads to an increase of the c/a ratio via an increase of the c parameter. As already commented, the c/a ratio in OVCs with DC structure is typically below 1.90 while the c/a ratio of OVCs with DS structure is typically above 1.97. Therefore, if we consider that the tetrahedral coordination of cations and anions is similar in both DS and DC phases, the increase of the unit cell volume in the DS phase with respect to the DC phase results in a smaller overlap between Ga and Se orbitals and consequently in a smaller direct bandgap energy compared to that of the DC phase.

The enlargement of the unit cell volume due to disorder produces the decrease of the direct bandgap energy. This effect is contrary to the effect of increasing pressure, which leads to a decrease of the unit cell volume, and consequently yields a larger overlap of cation and anion orbitals, and usually to an increase of the direct bandgap energy with increasing pressure. In our previous study of $CdGa_2Se_4$, we measured a considerable decrease of the pressure coefficient of the direct bandgap between DC and

DZ phases **[35]**. In this respect, we must note that further evidence of the difference between DS and DC phases of $ZnGa_2Se_4$ is given by the different pressure coefficient of the direct bandgap measured in both DS and DC phases which will be published elsewhere.

V. CONCLUSIONS

We have performed Raman scattering and optical absorption measurements in defect stannite (DS) $ZnGa_2Se_4$ subjected to controlled thermal annealing. We have found that an ordering of the cation substructure occurs during heating to 400ºC after 10 h leading to the crystallization of the defect chalcopyrite (DC) structure. We have shown that the DC structure can be retained on cooling at ambient temperature at a rate of the order of 1ºC/min. The Raman spectra at ambient conditions of the DS and DC structures of $ZnGa_2Se_4$ are discussed in detail emphasizing their similarities and differences. Both DC and DS structures have different properties. In particular, optical absorption measurements show that the DC phase has a larger direct bandgap energy than the DS phase.

Therefore, this work shows that minor changes in the cooling rate during the growth process of $ZnGa_2Se_4$ leads this material to be prepared in one of two different structures (DC or DS). This work allows explaining that the subtle differences found in the literature for $ZnGa_2Se_4$ are likely due to the different properties of DS- and DC-$ZnGa_2Se_4$. The observation of different properties in this material and the lack of knowledge of the detailed crystalline structure and of the exact conditions of the growth procedure have caused a misunderstanding in the scientific community and avoided the practical use of this material with non-linear optical properties in several technological applications. We hope this work will stimulate further work in this interesting compound.

References

[1] A. MacKinnon, in Tables of Numerical Data and Functional Relationships in Science and Technology, edited by O. Madelung, M. Schulz, and H. Weiss, Landolt-Börnstein New Series, Group III, Vol. 17, pt. h (Springer-Verlag, Berlin, 1985) p. 124.

[2] A.N. Georgobiani, S.I. Radautsan, and I. M. Tiginyanu, Fiz. Tekh. Poluprovodn. **19**, 193 (1985) [Sov. Phys. Semicond. **19**, 121 (1985)].

[3] J.E. Bernard and A. Zunger, Phys. Rev. B **37**, 6835 (1988).

[4] X. Jiang and W.R.L. Lambrecht, Phys. Rev. B **69**, 035201 (2004).

[5] I.S. Yahia, M. Fadel, G.B. Sakr, and S.S. Shenouda, J. Alloys and Comp. **507**, 551 (2010).

[6] I.S. Yahia, M. Fadel, G.B. Sakr, F. Yakuphanoglu, S.S. Shenouda, and W.A. Farooq, J. Alloys and Comp. **509**, 4414 (2011).

[7] H. Hahn, G. Frank, W. Klinger, A.D. Stórger, G. Stórger, Z. Anorg. Allg. Chem. **279**, 241 (1955).

[8] D. Errandonea, R.S. Kumar, F.J. Manjon, V.V. Ursaki and I.M. Tiginyanu, J. Appl. Phys. **104**, 063524 (2008).

[9] T. Hanada, F. Izumi, Y. Nakamura, O. Nittono and Q. Huang, Physica B **241–243**, 373 (1998).

[10] M.C. Morón and S. Hull, Phys. Rev. B **67**, 125208 (2003).

[11] M.C. Morón and S. Hull, J. Appl. Phys. **98**, 013904 (2005).

[12] M.C. Morón and S. Hull, J. Appl. Phys. **102**, 033919 (2007).

[13] G. Antonioli, P.P. Lottici and C. Razzetti, Phys. Status Solidi B **152**, 39 (1989).

[14] H. Hauseler, J. Solid State Chem. **26**, 367 (1978).

[15] A. Eifler, G. Krauss, V. Riede, V. Krämer and W. Grill, J. Phys. Chem. Solids **66**, 2052 (2005).

[16] I.M. Tiginyanu, V.V. Ursaki, and V.N. Fulga, Fiz. Tekh. Poluprovodn. **23**, 1725 (1989) [Sov. Phys. Semicond. **23**, 1069 (1989)].

[17] P.P. Lottici and C. Razzetti, Solid State Commun. **46**, 681 (1983).

[18] C. Razzetti, P.P. Lottici and G. Antonioli, Prog. Cryst. Growth and Charact.**15**, 43 (1987).

[19] G. Attolini, S. Bini, P.P. Lottici and C. Razzetti, Cryst. Res. Technol. **27**, 685 (1992).

[20] C. Razzetti and P.P. Lottici, Jpn. J. Appl. Phys. **32**, Suppl. 32-3, 431 (1993).

[21] V.V. Ursaki, I.I. Burkalov, I.M. Tiginyanu, Y.S. Raptis, E. Anastassakis and A. Aneda, Phys. Rev. B **59**, 257 (1999).

[22] K. Allakhverdiev, F. Gashimzade, T. Kerimova, T. Mitani, T. Naitou, K. Matsuishi and S. Onaric, J. Phys. Chem. Solids **64**, 1597 (2003).

[23] P. Alonso-Gutiérrez, Ph.D. thesis, *Estudio mediante espectroscopía Raman de la serie de semiconductores tetraédricos $Zn_{1-x}Mn_xGa_2Se_4$*, Colección de Estudios de Física, vol. 78 (Prensas Universitarias de Zaragoza, Zaragoza (Spain), 2009).

[24] P. Alonso-Gutiérrez, M.L. Sanjuán and M.C. Morón, Phys. Status Solidi (c) **6**, 1182 (2009).

[25] D. Caldera, M. Morocoima, M. Quintero, C. Rincon, R. Casanova and P. Grima, Solid State Commun. **151**, 212 (2011).

[26] H. Schwer, Thesis, Universität Freiburg, 1990.

[27] O. Gomis, R. Vilaplana, F.J. Manjón, E. Pérez-González, J. López-Solano, P. Rodríguez-Hernández, A. Muñoz, D. Errandonea, J. Ruiz-Fuertes, A. Segura, D. Santamaría-Pérez, I.M. Tiginyanu, and V.V. Ursaki, J. Appl. Phys. **111**, 013518 (2012).

[28] A. Eifler, J.-D. Hecht, G. Lippold, V. Riede, W. Grill, G. Krauss, and V. Krämer, Physica B **263-264**, 806 (1999).

[29] J.C. Woolley, R. Brun del Re and M. Quintero, Phys. Status Solidi A **159**, 361 (1997).

[30] M.L. Sanjuán and M.C. Morón, Physica B **316-317**, 565 (2002).

[31] I.M. Tiginyanu, N.A. Modovyan, and O.D. Stoika, Sov. Phys. Solid State **34**, 527 (1992).

[32] R. Letoullec, J. P. Pinceaux, and P. Loubeyre, High Press. Res. **1**, 77 (1988).

[33] G. Kresse et al, computer code VASP; see http://www.vasp.at

[34] J. P. Perdew , K. Burke and , M. Ernzerhof, Phys. Rev. Lett. **78**, 1396 (1997).

[35] F.J. Manjón, O. Gomis, P. Rodríguez-Hernández, E. Pérez-González, A. Muñoz, D. Errandonea, J. Ruiz-Fuertes, A. Segura, M. Fuentes-Cabrera, I.M. Tiginyanu, and V.V. Ursaki, Phys. Rev. B **81**, 195201 (2010).

[36] D. Santamaría-Pérez, M. Amboage, F.J. Manjón, D. Errandonea, A. Muñoz, P. Rodríguez-Hernández, A. Mujica, S. Radescu, V.V. Ursaki and I.M. Tiginyanu, J. Phys. Chem. C **116**, 14078 (2012).

[37] K. Parlinski, computer code PHONON. See:
http://www.computingformaterials.com/index.html.

[38] S. Baroni, S. Gironcoli, A. del Corso and P. Giannozzi, Rew. Of Mod. Physics, 73, 515 (2001).

[39] P. Giannozzi, S. Baroni, P. Bonini, et al., J. Phys.:Condens. Matter 21 395502 (2009).

[40] E. Kroumova, M.I. Aroyo, J.M. Perez-Mato, A. Kirov, C. Capillas, S. Ivantchev, and H. Wondratschek, Phase Transitions **76**, 155 (2003).

[41] R. Loudon Adv. Phys. 13, 423 (1964).

[42] P. Alonso-Gutiérrez and M.L. Sanjuán, Phys. Rev. B **78**, 045212 (2008).

[43] F.J. Manjón, B. Marí, J. Serrano, and A.H. Romero, J. Appl. Phys. **97**, 053516 (2005).

[44] P. Alonso-Gutiérrez, M.L. Sanjuán, M.C. Morón, Physics of Semiconductors, AIP Conf. Proc 893 parts A and B, **185** (2007).

[45] L. Garbato, F. Ledda, and A. Rucci, Prog. Cryst. Growth Charact. **15**, 1 (1987).

[46] A. Grzechnik, V.V. Ursaki, K. Syassen, I. Loa, I.M. Tiginyanu, and M. Handfland, J. Solid State Chem. **160**, 205 (2001).

[47] J. Marquina, Ch. Power, P. Grima, M. Morocoima, M. Quintero, B. Couzinet, J.C. chervin, P. Munsch, and J. González, J. Appl. Phys. **100**, 093513 (2006).

[48] S. Meenakshi, V. Vijyakumar, A. Eifler, and H. D. Hochheimer, J. Phys. Chem. Solids **71**, 832 (2010).

[49] O. Gomis, R. Vilaplana, F.J. Manjón, D. Santamaría-Pérez, J. Ruíz-Fuertes, D. Errandonea, E. Pérez-González, J. López-Solano, P. Rodríguez-Hernández, A. Muñoz, I. M. Tiginyanu, and V. V. Ursaki, sent for publication.

[50] C. K. Lowe-Ma and T.A. Vanderah, Acta Cryst. C **47**, 919 (1991).

[51] L. Roa, J. C. Chervin, A. Chevy, M. Davila, P. Grima, and J. González, Phys. Stat. Solidi (b) **198**, 99 (1996).

Table 1: Experimental (exp.) and calculated (th.) frequencies of first-order Raman modes in DS-$ZnGa_2Se_4$ at ambient conditions.

Mode symmetry (th.)	ω_0 (th.)[a] (cm^{-1})	Mode symmetry (exp.)	ω_0 (exp.)[a] (cm^{-1})	ω_0 (exp.)[b] (cm^{-1})	ω_0 (exp.)[c] (cm^{-1})
$E^1(TO)$	78.8	$E^1(TO)$			
$E^1(LO)$	79.3	$E^1(LO)$	82.6	84	84
B_1^1	90.8	B_1^1	92.7	90	92
$E^2(TO)$	107.4	$E^2(TO)$			
$E^2(LO)$	107.4	$E^2(LO)$	106.9	106	107.2
$B_2^1(TO)$	110.8	$B_2^1(TO)$			
$B_2^1(LO)$	115.7	$B_2^1(LO)$	126	126	125.6#
A_1^1	142.0	A_1^1	142.8	143	143.1
A_2	187.4	A_2 (silent)	182.6	180	
A_1^2	195.6	A_1^2	208.3	209	207.3
$B_2^2(TO)$	198.7	$E^3(TO)$			
$B_2^2(LO)$	206.6	$E^3(LO)$	196	180*	217.4
$E^3(TO)$	212.3	B_1^2	229.3		232.6+
$E^3(LO)$	215.4	$E^4(TO)$ + $B_2^2(TO)$	239.4	243	240
$E^4(TO)$	223.0			234	
$E^4(LO)$	226.3	$E^4(LO)$ + $B_2^2(LO)$	246.5	243	247.3
$E^5(TO)$	227.2			234	
$E^5(LO)$	258.5	$E^5(TO)$ + $B_2^3(TO)$	260.4		265.3
B_1^2	243.0				
$B_2^3(TO)$	268.8	$E^5(LO)$ + $B_2^3(LO)$	285.7	285	285.3
$B_2^3(LO)$	288.4				

[a] This work

[b] Ref. 21

[c] Ref. 23

* Authors in Ref. 21 assigned this Raman peak to the E^3 mode.

\# Authors in Ref. 23 assigned this Raman peak to a B_1 mode.

+ Authors in Ref. 23 assigned this Raman peak to a B_2 mode.

Table 2. Experimental (exp.) and calculated (th.) frequencies of first-order Raman modes in DC-ZnGa$_2$Se$_4$ at ambient conditions.

Mode symmetry (th.)	ω_0 (th.)[a] (cm^{-1})	Mode symmetry (exp.)	ω_0 (exp.)[a] (cm^{-1})	ω_0 (exp.) (cm^{-1})
E^1(TO)	79.3	E^1(TO)	82.0	82[b], 84[c]
E^1(LO)	80.0	E^1(LO)		
B^1(TO)	88.9	B^1(TO)	91.9	92.5[b], 94[c]
B^1(LO)	89.1	B^1(LO)		
E^2(TO)	101.0	E^2(TO)	105.8	106[b], 109[c]
E^2(LO)	101.1	E^2(LO)		
B^2(TO)	123.0	B^2(TO)	125.1	126[b], 128[c]
B^2(LO)	126.8	B^2(LO)		129[b]
A^1	140.1	A^1	141.9	143[b], 145[c]
A^2	182.8	A^2	188.4	182[b], 193[c]
E^3(TO)	197.6	E^3(TO)	194.7	190[b]
E^3(LO)	203.1	E^3(LO)		198[b]
A^3	197.3	A^3	207.9	210[b], 209[c]
B^3(TO)	218.4	B^3(TO)	229.2	222[b]
B^3(LO)	222.3	B^3(LO)		
B^4(TO)	221.7	E^4(TO) + B^4(TO)	239.3	233.5[b†], 235[c]
B^4(LO)	236.3			
E^4(TO)	232.5	E^4(LO) + B^4(LO)	244.2	241[b+], 242[c]
E^4(LO)	239.9			248[b+], 250[c]
E^5(TO)	245.5	E^5(TO) + B^5(TO)	259.0	
E^5(LO)	267.5			280.5[b]
B^5(TO)	253.8	E^5(LO) + B^5(LO)	281.3	260.5[b*], 263[c]
B^5(LO)	269.7			286.5[b*], 285[c]

[a] This work.

[b] Ref. 15.

[c] Ref. 16.

[†] Authors in Ref. 15. assigned this mode to the TO component of the B^4 mode.

[+] Authors in Ref. 15. assigned these modes to the TO and LO components of the E^4 mode.

[*] Authors in Ref. 15. assigned these modes to the TO and LO components of the B^5 mode.

Figure captions

Fig. 1. (Color online) Scheme of atoms in $ZnGa_2Se_4$ in defect chalcopyrite (DC) structure (a) and defect stannite (DS) (model 2 in Ref. 27) structure (b). Big (blue) atoms are Se, small (red) dark atoms are Ga, and small (magenta) light atoms are Zn. Mixed Ga and Zn atoms in DS structures are shown in rose color. For the sake of clarity Wyckoff sites are given in parenthesis.

Fig. 2. Unpolarized Raman spectra of $ZnGa_2Se_4$ during thermal annealing at different temperatures. Asterisk marks the strong new mode that appears after heating the DS sample at 400ºC for 10 h. This mode (A^2) is characteristic of the DC phase and it is absent in the DS phase. Note that the equivalent mode in the DS phase is the A_2 mode which is silent but can be observed by defect-assisted Raman scattering (see text).

Fig. 3. (Color online) Unpolarized RT Raman spectra of DS-$ZnGa_2Se_4$ (black, bottom) and DC-$ZnGa_2Se_4$ (red, top) in two different parts of the samples. Labels refer to symmetry assignments for the Raman modes in the DS and DC structures. *Ab-initio-*calculated values of the TO (solid) and LO (dotted) first-order Raman-active mode frequencies for both DS (DC) samples are marked with vertical black (red) marks at the bottom.

Fig. 4. Polarized RT Raman spectra taken in backscattering geometry along the (111) direction with crossed polarization in a direction close to [110] for as-grown DS-$ZnGa_2Se_4$ (black, bottom), after heating at 400 ºC for 10h resulting in DC-$ZnGa_2Se_4$ (red, top). Cooling rate was always 1ºC/min.

Fig. 5. RT optical absorption spectra of DS-$ZnGa_2Se_4$ (black) and DC-$ZnGa_2Se_4$ (red) samples. Arrows indicate the experimental direct bandgap energies in both phases.
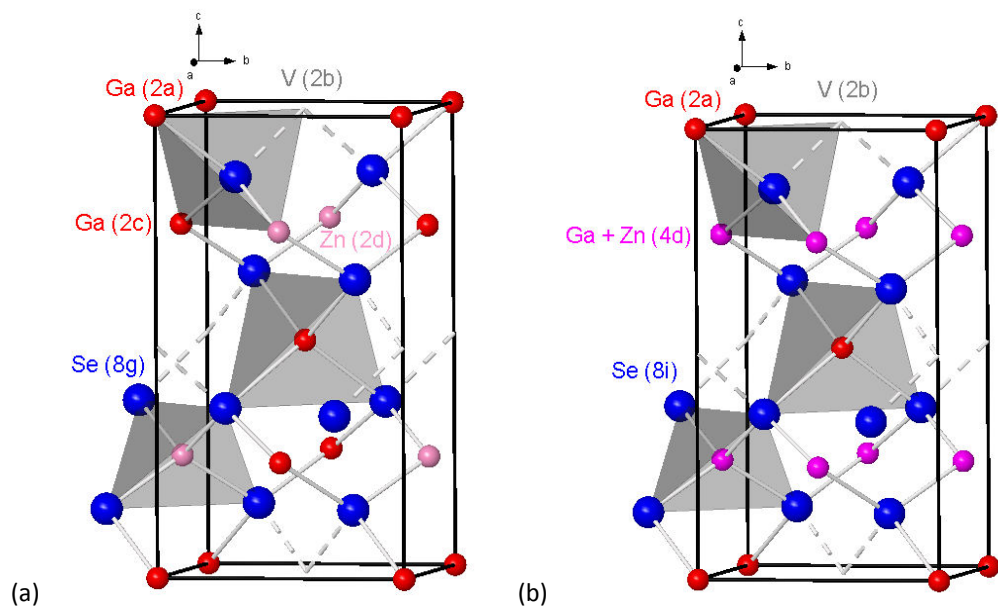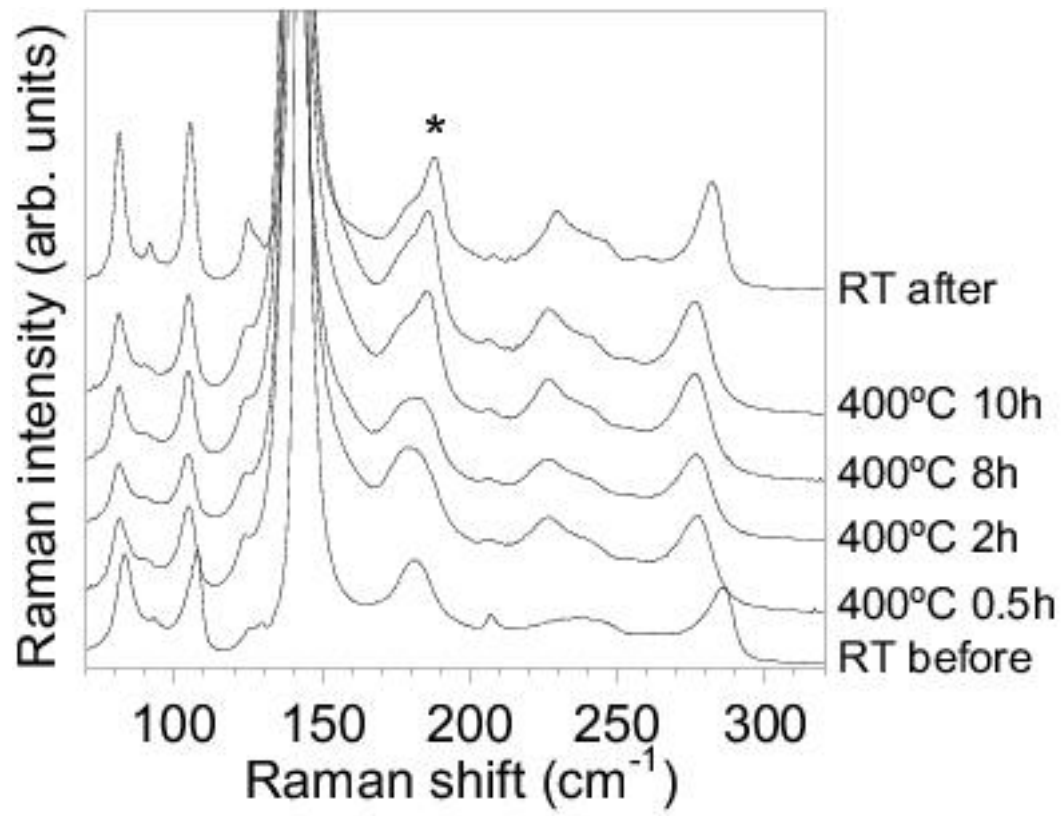
Fig. 1.

(a)
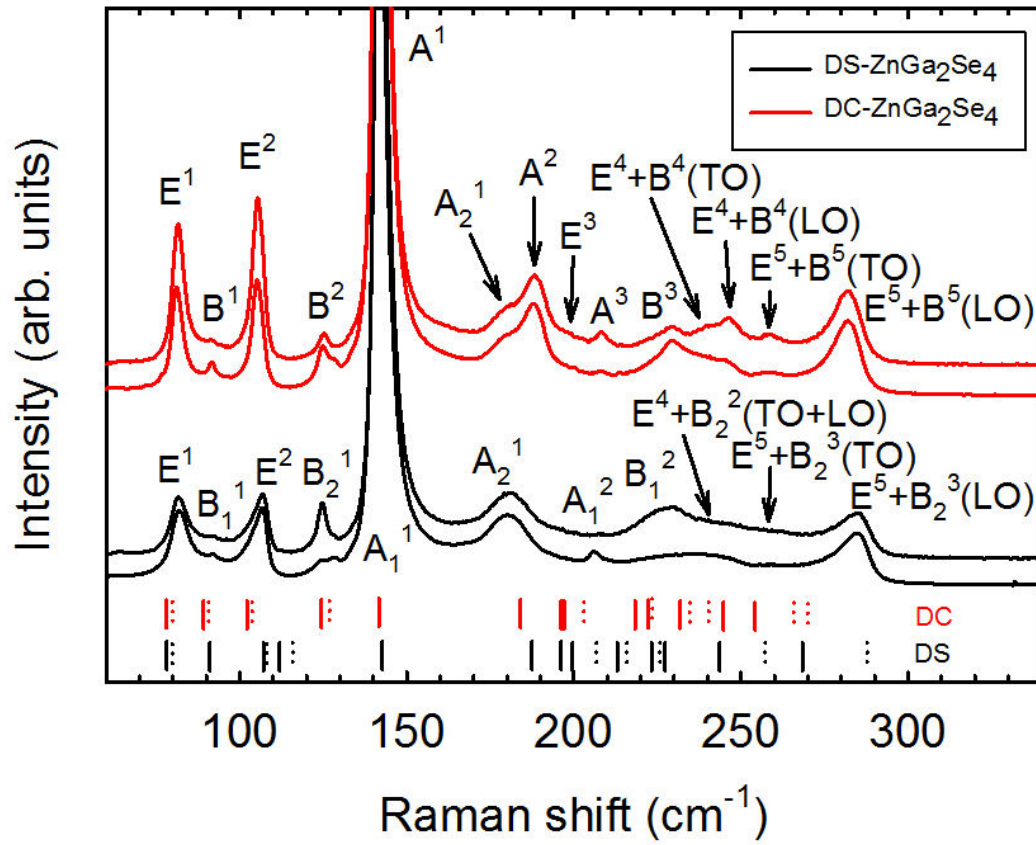
(b)

Fig. 2

Fig. 3

Fig. 4

Fig. 5